*Technology and Science for the Ships of the Future*
*V. Crupi and V. Bucci (Eds.)*


*doi:10.3233/PMST250006*

# Nonlinear Model-Based Control of a Gyroscopic Stabilization System for High-Speed Crafts

Gianluca PEPE[a], Maicol LAURENZA[b], Giacomo FEDERICI[a], Silvia MILANA[a] and Antonio CARCATERRA[a]
[a] *Department of Mechanical and Aerospace Engineering, University of Rome La Sapienza, Rome, Italy*
[b] *Department of Engineering, Niccolò Cusano University, Rome, Italy*

**Abstract.** The growing demand for stability in high-speed vessels has driven the development of advanced gyroscopic systems to reduce roll motion and improve passenger comfort. This work proposes a model-based nonlinear control approach applied to an active gyroscopic stabilizer installed on a semi-displacement catamaran. A 10-degree-of-freedom dynamic model has been developed, 6 for the vessel and 2 for each pair of gyroscopes, encompassing metacentric buoyancy forces and comprehensive scenarios that account for hydrodynamic actions, wind, waves, and propulsion. The control system adopts the FLOP strategy (Feedback Local Optimality Principle), which optimizes the gyroscopes' precession and spin speed in real time to adaptively counteract roll motions and, to a lesser extent, pitch, thereby reducing local accelerations. Simulations conducted under various sea conditions (Beaufort 2–4) show up to an 80% reduction in roll amplitude, along with up to a 40% improvement in motion sickness incidence (MSI) evaluated in accordance with ISO 2631. Additionally, the FLOP controller outperforms passive gyroscopic systems and a traditional PID in terms of stability, maintaining modest power demands even in the presence of resonant frequencies and nonlinear wave interactions. Finally, an energy analysis has been carried out to assess the power required for installing the gyroscopic system, considering the added displacement and resulting hydrodynamic resistance, as well as the power needed for active precession control and spin speed regulation, considering the benefits gained in stability and comfort.

**Keywords.** Gyrostabilizer, Optimal variational control, Motion sickness incidence

## 1. Introduction

The dynamic stability of high-speed vessels in open water is a critical issue for onboard safety and comfort. Excessive roll and pitch can compromise not only the vessel's operability, but in extreme situations may even threaten its very survival, in addition to making maneuvers difficult and causing significant discomfort or seasickness among crew and passengers [1]. In particular, wave-induced vibrations on the vessel can easily exceed the comfort thresholds established by international standards such as ISO 2631, which concerns whole-body vibrations [2, 3]. Consequently, the effective reduction of these motions through active control systems is essential for enhancing navigational safety and occupant comfort, especially in high-speed craft used for critical operations.

Traditionally, both passive and active solutions have been adopted to mitigate roll and pitch, each with significant limitations. External anti-roll devices—such as stabilizing fins, winglets, or other hull appendages—generate hydrodynamic forces to counteract roll but prove ineffective at low speeds or when the vessel is stationary, in addition to increasing drag [4]. In contrast, internal systems, such as anti-roll tanks or gyroscopes, act from within without altering the hull's form. In particular, a gyroscopic stabilizer uses a rapidly spinning flywheel whose precession generates a moment opposing the vessel's roll [5]. Unlike fins, gyroscopes do not increase hydrodynamic resistance and remain effective both when the hull is stationary and at all speeds, a particularly important aspect for high-speed vessels. Early active gyroscopes—for example, the Sperry prototypes installed on yachts in 1915—already demonstrated roll reductions of up to 95% (RMS) under favourable conditions. However, mechanical complexity, high costs, and the lack of sophisticated control algorithms limited their widespread adoption for many decades [6]. In practice, classical tuning with linear controllers (e.g., PID) can mitigate roll but often yields suboptimal performance in rough seas and when faced with strongly nonlinear dynamics [7, 8]. In recent years, thanks to advancements in materials and technologies, naval gyroscopes have regained interest. Recent experimental tests on ship models have shown roll reductions of around 50% even with basic conventional controls [9], suggesting there is considerable room for improvement by adopting more advanced control strategies that fully exploit the gyroscope's potential [10]. Indeed, recent studies confirm that advanced approaches—such as Model Predictive Control (MPC)—can achieve roll reductions of over 90% in various wave scenarios [6, 11], without exceeding the device's physical limits.

Considering the above, this research proposes an innovative approach to active control of a gyroscopic stabilizer for high-speed vessels. The approach is based on advanced nonlinear control that employs a complete 6-degree-of-freedom (6-DOF) dynamic model for the vessel, plus 2 degrees of freedom for each gyroscope installed onboard. Unlike simplified single-DOF models, which are often limited to roll alone [12], the use of a 6-DOF model captures the interaction between roll, pitch, and the vessel's other motions, improving the prediction of system behaviour under various operating conditions. The designed control algorithm, called the Feedback Local Optimality Principle (FLOP) [13, 14], is based on a variational principle that integrates the dynamics of both the vessel and the gyroscope, effectively managing the strong nonlinearities arising from their dynamic coupling. Compared to a control approach based on linear models, the proposed strategy adapts to a broader range of sea conditions and actuation constraints, guaranteeing greater roll attenuation. In accordance with ISO 2631, a simulation campaign is conducted to assess how the gyroscopic stabilization system influences motion sickness perception by evaluating objective metrics such as the reduction of Root Mean Square (RMS) vertical/angular acceleration, weighted according to the standard. Its effectiveness in reducing oscillations under various sea states is compared against the vessel without a gyroscope, a gyroscope installed but without active precession control, a PID control, and finally the results achieved using the FLOP control approach.

## 2. Configuration of the stabilization system on a passenger catamaran

The stabilization system has been implemented on a hydrofoil configured as a catamaran, specifically designed for passenger transport (Figure 1). The reference vessel, with a gross tonnage of 400 tons, a net tonnage of 280 tons, and a summer payload of 50 tons, has dimensions including an overall length ($L_{OA}$) of 36 meters, a length between perpendiculars ($L_{pp}$) of 27 meters, a beam of 9.5 meters, a construction height of 3.5 meters, and a maximum draft of 1.3 meters. The main engine consists of two diesel units for a total power of about 3.8 kW, while propulsion is provided by two waterjets, allowing the vessel to reach a maximum speed of 32 knots and accommodate up to 318 passengers.

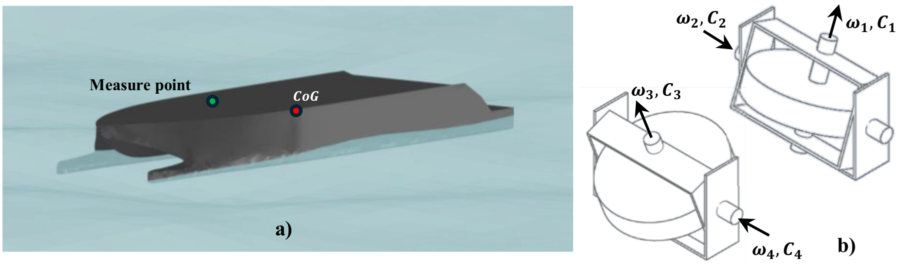


**Figure 1.** On the left **a**), a schematic view of the catamaran showing the measurement point for the whole-body accelerations (used to compute the MSI) and the sea surface as a reference. On the right **b**), a diagram of the two-degree-of-freedom gyroscopic platforms (precession and spin) installed on vessel.

For the calculation of the coefficients of the added mass matrix and potential damping, the software Ansys AQWA was used. This software employs a first-order potential flow theory and discretizes the structure's surface into panel elements to solve diffraction and radiation problems, thus determining the hydrodynamic loads associated with wave motion (Table 1). The stabilizing gyroscope examined generates a gyroscopic moment that counteracts the roll induced by waves on the hull; internally, a high-speed flywheel supported by a single gimbal experiences an excitation moment proportional to the roll rate, which causes a change in angular momentum and the consequent precession of the flywheel. The resulting moment, obtained from the combination of the rotational speed and the precession rate, is used to reduce the undesired motion. In particular, the configuration with two counter-rotating Veem VG70 Mark II gyroscopes (Table 1) was analyzed, which guarantees a greater ability to maintain course compared to a single device, as the torque generated by one on the yaw axis is compensated by the action of the other, canceling the unwanted moments related to pitch and yaw while doubling the control moment on roll.

**Table 1.** Hydrodynamic parameters of the vessel, according to Fossen's nomenclature [15], and specifications of the gyro stabilization system. The main ship parameters are computed via commercial software Ansys AQWA with academic licensing.

| Main Ship parameters | | | | Gyro VG70 Mark II | |
|---|---|---|---|---|---|
| $\boldsymbol{A}_{11}(0)$ | 3220 kg | $\boldsymbol{B}_{44}(\omega_{n,roll})$ | $1.23\cdot10^6$ Nms | **Angular moment** | 70 kNms |
| $\boldsymbol{A}_{22}(0)$ | $93.4\cdot10^3$ kg | $\boldsymbol{B}_{55}(\omega_{n,pitch})$ | $4.92\cdot10^6$ Nms | **Nominal torque** | 145 kNm |
| $\boldsymbol{A}_{33}(\omega_{n,z})$ | $102\cdot10^3$ kg | $\omega_{n,z}$ | $0.4\cdot2\pi$ rad/s | **Dimension** | 1650 x 1590 x 1200 mm |

| | | | | | |
|---|---|---|---|---|---|
| $\boldsymbol{A}_{44}(\omega_{n,roll})$ | 2.53·10$^6$ $kgm^2$ | $\omega_{n,roll}$ | 0.35·2$\pi$ rad/s | **Mass** | 2850 kg |
| $\boldsymbol{A}_{55}(\omega_{n,pitch})$ | 7.88·10$^6$ $kgm^2$ | $\omega_{n,pitch}$ | 0.39·2$\pi$ rad/s | **Max power** | 18 kW |
| $\boldsymbol{A}_{66}(0)$ | 9.05·10$^6$ $kgm^2$ | $GM_t$; $GM_l$ | 16.7 m ; 94 m | **Rotor RPM** | 4800 rpm |
| $\boldsymbol{A}_{26}(0)$ | 16700 Nm | $\boldsymbol{B}_{33}(\omega_{n,z})$ | 67200 Nms | | |

The installation position does not affect the effectiveness of the gyroscopes. In the tests, the two devices were placed along the fore-aft axis, symmetrically with respect to the center of gravity. However, their presence increases the displacement and modifies the added mass and damping parameters, resulting in increased hydrodynamic resistance and, therefore, higher energy consumption. In fact, the resistance curve changes and the mechanical power required for motion increases: for example, at 16 m/s, the installation of a gyroscope results in an approximate 4% increase in the required power. Finally, the system can be classified into two types, passive and active: in the passive gyroscope, the undesired moment is spontaneously neutralized through precession, whereas in the active system, the gyroscope is controlled by a controller that acts on both precession and spin, generating higher-intensity correction torques. In the results section, the different configurations will be compared: the passive system, the active system managed via PID control, and the FLOP control system.

## 3. Dynamic model of the vessel for gyroscopic control

In studying the gyroscopic stabilizing action on a vessel, it is fundamental to adopt a model capable of accurately describing the dynamics of the craft. To this end, the nonlinear 6DOF maneuvering model proposed by Fossen [15] is used, which is expressed by the following equations:

$$\begin{cases} \boldsymbol{M}_{RB}\dot{\boldsymbol{v}} + \boldsymbol{C}_{RB}(\boldsymbol{v})\boldsymbol{v} = \boldsymbol{\tau}_h + \boldsymbol{\tau}_a + \boldsymbol{\tau}_w + \boldsymbol{\tau}_s + \boldsymbol{\tau}_g \\ \boldsymbol{M}_G(\phi)\dot{\boldsymbol{\omega}} + \boldsymbol{C}_G(p, \boldsymbol{\omega})\boldsymbol{\omega} = \boldsymbol{u} \\ \dot{\boldsymbol{\eta}} = \boldsymbol{R}(\psi)\boldsymbol{v} \end{cases} \quad (1)$$

where the velocity vector $\boldsymbol{v} = [u, v, w, p, q, r]^{\mathrm{T}}$ represents, respectively, the surge, sway, heave, and the roll, pitch, and yaw rates, while the vector $\boldsymbol{\eta} = [x, y, z, \phi, \theta, \psi]^{\mathrm{T}}$ describes the position and orientation in the inertial frame. The matrix $\boldsymbol{M}_{RB}$ represents the rigid-body inertia, $\boldsymbol{C}_{RB}(\boldsymbol{v})$ the Coriolis effects, and $\boldsymbol{R}(\psi)$ is the rotation matrix that transforms the body-fixed frame into the inertial frame.

The forces acting on the system are divided into several categories, including hydrodynamic and hydrostatic effects, indicated by $\boldsymbol{\tau}_h$ and $\boldsymbol{\tau}_a$; environmental forces due to wind and waves, represented by $\boldsymbol{\tau}_w$ and $\boldsymbol{\tau}_s$; and the gyroscopic actions $\boldsymbol{\tau}_g$. In particular, the hydrodynamic actions arise from the interaction with water when a relative motion $\boldsymbol{v}_r = \boldsymbol{v} - \boldsymbol{v}_c$ is established due to the current, and they include the linear and nonlinear viscous damping as well as the hydrodynamic resistance in terms of an added mass matrix and added Coriolis effects: $\boldsymbol{\tau}_h = -(\boldsymbol{M}_A\dot{\boldsymbol{v}} + \boldsymbol{C}_A(\boldsymbol{v}_r)\boldsymbol{v}_r + \boldsymbol{D}_l\boldsymbol{v}_r + \boldsymbol{D}_n(\boldsymbol{v}_r)\boldsymbol{v}_r)$. The hydrostatic forces, on the other hand, are modeled using the metacentric concept, where the hydrostatic forces and moments act as elastic restoring forces that tend to bring the vessel back to an equilibrium position [15]. The Airone Jet, classified as a semi-displacement vessel, exhibits particular characteristics in this regard. At low speeds, the vessel's dynamics are primarily governed by these hydrostatic effects. However, when the vessel reaches high speeds, planing effects must also be considered. Under these conditions, the vessel begins to partially lift out of the water, generating a lift force along the z-axis and a moment about the pitch axis. To analyze and predict these effects, the Savitsky theory is used, which provides a detailed model to quantify both the lift and the forces and moments associated with the planing phenomenon [15].

In addition, the wind actions are modeled by a mean component and a turbulent component, the latter characterized by the NPD – Norwegian Petroleum Directorate spectrum [16], while the wave elevation is described as a sum of sinusoids with random phase according to the Pierson–Moskowitz spectrum [15].

The gyroscopic actions, which are fundamental for influencing the ship's attitude, are calculated through a dynamic model that provides control over both the spin angle and the precession. In this context, the vector $\boldsymbol{\omega} = [\omega_1, \omega_2, \omega_3, \omega_4]$ comprises the spin angular velocities $\omega_1, \omega_3$ and the precession rates $\omega_2, \omega_4$ of the two gyroscopes, while the mass matrix $\boldsymbol{M}_G$ and the Coriolis matrix $\boldsymbol{C}_G$ depend directly on the vessel's roll, expressed by $\phi$ and the roll rate $p$. The control action $\boldsymbol{u} = [C_1, C_2, C_3, C_4]$ represents the torques to be applied on the spin axes, to maintain a constant rotational speed, and on the precession axis, in order to generate the stabilizing moment $\boldsymbol{\tau}_g$ on the vessel.

To determine the gyroscopic actions necessary to reduce the vessel's roll, a nonlinear model-based control called FLOP – Feedback Local Optimality Control – has been implemented. The control technique developed by the authors belongs to the class of variational controls, but it uses a principle of local rather than global optimality, thus allowing for a feedback control law without the constraint of employing a quadratic cost function and a linear dynamic model. In this context, the dynamic model, which must be affine, is expressed from (1) as $\dot{\boldsymbol{x}} = \boldsymbol{\phi}(\boldsymbol{x}) + \boldsymbol{B}\boldsymbol{u}$, with $\boldsymbol{x} = [\boldsymbol{\nu}, \boldsymbol{\omega}, \boldsymbol{\eta}]$.

$$\boldsymbol{\phi}(\boldsymbol{x}) = \begin{bmatrix} \boldsymbol{M}_{RB}^{-1}\left(\boldsymbol{\tau}_h + \boldsymbol{\tau}_a + \boldsymbol{\tau}_w + \boldsymbol{\tau}_s + \boldsymbol{\tau}_g - \boldsymbol{C}_{RB}(\boldsymbol{\nu})\boldsymbol{\nu}\right) \\ \boldsymbol{M}_G^{-1}\boldsymbol{C}_G\boldsymbol{\omega} \\ \boldsymbol{R}(\psi)\boldsymbol{\nu} \end{bmatrix} \quad \boldsymbol{B} = \begin{bmatrix} \boldsymbol{0}_{6x4} \\ \boldsymbol{M}_G^{-1} \\ \boldsymbol{0}_{3x4} \end{bmatrix} \tag{2}$$

The FLOP principle is based on minimizing the objective function

$$J = \int_0^T \frac{1}{2}\, \boldsymbol{u}^{\boldsymbol{T}}\boldsymbol{R}\boldsymbol{u} + g(\boldsymbol{x}) + \boldsymbol{\lambda}^T\left(\dot{\boldsymbol{x}} - (\boldsymbol{\phi}(\boldsymbol{x}) + \boldsymbol{B}\boldsymbol{u})\right)dt \tag{3}$$

where $\boldsymbol{R}$ is the tuning matrix to regularize the control actions $\boldsymbol{u}$ and $\boldsymbol{\lambda}$ is the Lagrange multiplier that enforces the dynamic constraint. The function $g(\boldsymbol{x})$ is nonlinear and differentiable with respect to the state x; it allows for imposing limits on the precession angle, preventing it from approaching too close to 90° or –90°, angles that would make device control difficult and compromise system effectiveness. The method allows deriving an explicit control law by exploiting discrete approximations for the solution of the differential system, in which the transversal boundary conditions are handled according to the classical Pontryagin optimal control approach. For more details, see [17, 18].

$$\boldsymbol{u} = \boldsymbol{R}^{-T}\boldsymbol{B}^T\left(\left[\nabla_x\boldsymbol{\phi}^T - \frac{1}{\Delta\tau}\boldsymbol{I}\right]^{-1}\nabla_x g\right) \tag{4}$$

The terms $\nabla_x \boldsymbol{\phi}$ and $\nabla_x g$ represent the Jacobian of the nonlinear component of the dynamics and of $g(\boldsymbol{x})$ with respect to the state $x$, and $\Delta\tau$ is a time interval chosen ad hoc to set the control's prediction capabilities. Furthermore, the control system considers the maximum actuation limits in terms of power, speed, and maximum torques, as reported in Table 1.

## 4. Numerical simulations for comfort evaluation and roll reduction

According to ISO 2631, the risk of seasickness is assessed by measuring vibrations along the vessel's main axes, with particular focus on the vertical axis since it has the greatest impact on balance and motion perception by the human body. The collected data are filtered using weighting curves, which reflect the physiological response to critical vibration frequencies, typically ranging from 0.1 to 0.5 Hz [19, 20]. After filtering, the weighted acceleration $a_w$, is obtained, representing the RMS (Root Mean Square) value calibrated to the human response to seasickness. For continuous exposure at a constant intensity, the Motion Sickness Dose Value (MSDV) is calculated using $MDSV = a_w\, T_0^{1/2}$ where $T_0$ is the duration of exposure (20 minutes in this case). Based on this parameter, the Motion Sickness Incidence (MSI), the percentage of individuals susceptible to vomiting, is then determined by $MSI = 0.33\, MSDV$.
This relationship is suitable for representing a general adult population (including both males and females), as it converts a physical parameter (MSDV) into an estimate of health impact, indicating how many individuals may experience discomfort symptoms. The resulting estimation function is embedded into the FLOP control cost function through $g(\boldsymbol{x})$. In this way, the control algorithm is explicitly designed to minimize the MSI index, even though the relationship itself is nonlinear.

Within the framework of a comprehensive evaluation of the control system's performance, multiple simulation scenarios were defined by varying sea and wind conditions. In particular, the case of Sea State 4 was studied, where the peak wave frequency coincides with the ship's natural frequencies (approximately 0.3 Hz), thereby maximizing the resonance effect. The sea model is described by the Pierson-Moskowitz spectrum, which calculates the peak frequency $\omega_p$ based on the wind speed measured at 19.5 meters, according to the relation $\omega_p = 0.877 g / U_{19.5}$. The effective excitation frequency $\omega_e$ is then corrected based on the vessel's speed $V$, using the formula $\omega_e = \omega_p - \left(\omega_p^2 / g\right) V$, resulting in a critical advance speed of about 12 m/s. In this way, the encounter frequency of the waves aligns with the vessel's natural frequencies (roll, pitch, and heave), putting the control system's stabilizing capabilities under stress.

Figure 2a presents the roll reduction results, comparing four configurations: without a gyroscopic system (in blue), with a passive gyroscopic system that maintains only a constant spin speed (in orange), with a simple PID control for the precession angle (in green), and with FLOP control (in light blue). The data show that the passive system alone is able to significantly reduce the oscillations, up to 53% in the case of Sea State 2, while its effectiveness decreases under Sea State 4 conditions. The adoption of an active system, such as FLOP control, allows for reductions up to 83% under moderate conditions; however, even in this case, performance in Sea State 4 is limited, with a maximum reduction of 18%. In cases of particularly intense sea and wind conditions, the gyroscopic system installed on the catamaran reaches the limits of the maximum torque it can generate, causing the control to saturate and reducing its effectiveness. Although larger gyroscopes could potentially provide a higher angular moment, implementing bulkier or heavier solutions is impractical for the configuration under study.

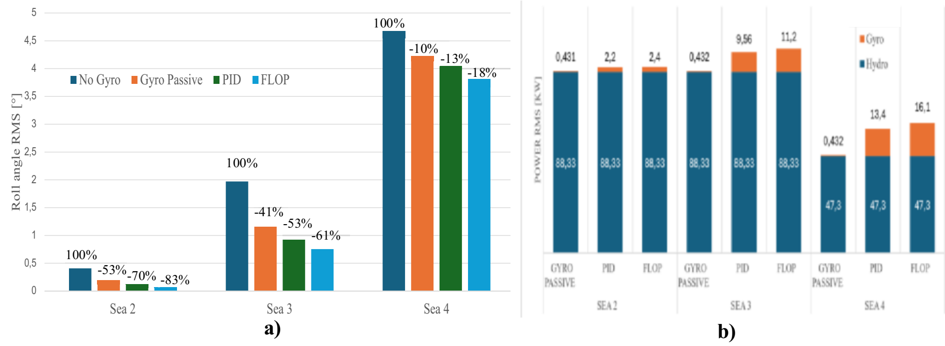


**Figure 2.** Roll reduction in the three cases of sea state 2, 3, and 4: absence of the gyroscopic system in blue, passive system in orange, PID control in green, FLOP control in light blue **a**); Power consumption due to the increase in hydrodynamic resistance caused by the presence of the gyroscope system (blue); power consumption for the gyroscopic stabilization (orange). The ship travels at 16 m/s in Sea State 2 and 3, and at 12 m/s in Sea State 4 **b**).

Figure 2b shows the power consumed under various environmental conditions and control configurations. The blue power represents the energy required to cope with the increased hydrodynamic resistance due to the additional onboard mass, while the orange power indicates the share absorbed by the gyroscope. It is evident that the passive system, which uses power solely to maintain a constant spin speed, consumes a minimal amount, equal to 0.432 kW. In contrast, the active systems require increasingly higher power as sea conditions worsen, reaching up to 16.1 kW in the case of FLOP control. The latter, in fact, fully exploits the available power to achieve a greater reduction in oscillations, even in extreme situations, naturally leading to higher energy consumption.

Finally, Figure 3 shows the percentage of passengers experiencing seasickness after 20 minutes of exposure, measured at a point on the vessel with coordinates in meters [8, -4, 0] relative to the center of gravity. This position was chosen to include the combined effect of the vertical (heave) component and the pitch and roll rotations. In Sea State 2 conditions, the reduction in roll is not sufficient to alleviate seasickness, as the vertical accelerations, which are not controllable by the gyroscopes, are predominant. In contrast, under Sea State 3 and 4 conditions, FLOP control outperforms PID in reducing discomfort, also demonstrating good control stability when the excitation approaches the vessel's natural frequencies.

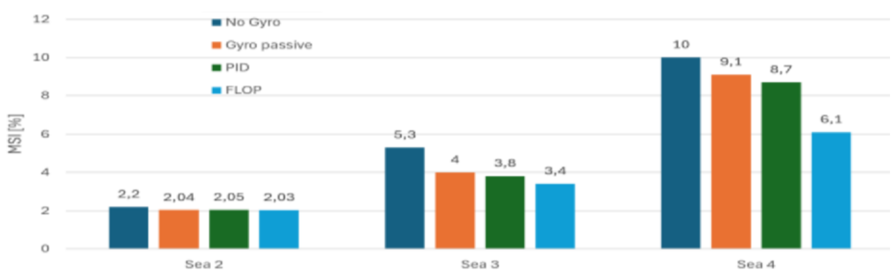


**Figure 3.** Percentage of passenger seasickness after 20 min.

## References


[1] D. Vassalos and D. Paterson, "Towards unsinkable ships," Ocean Engineering, vol. 232, p.

[2] F. Roshan, A. Dashtimanesh, and P. Kujala, "Safety Improvements for High-Speed Planing Craft Occupants: A Systematic Review," Journal of Marine Science and Engineering, vol. 12, no. 5, doi: 10.3390/jmse12050845.

[3] A. Lawther and M. J. Griffin, "Motion sickness and motion characteristics of vessels at sea," Ergonomics, vol. 31 10, pp. 1373-94, 1988.

[4] R. Li, T. Li, W. Bai, and X. Du, "An adaptive neural network approach for ship roll stabilization via fin control," Neurocomputing, vol. 173, pp.

[5] B. Li, X. Zhang, J. Wang, and N. Chen, "Anti-Roll Characteristics of Marine Gyrostabilizer Based on Adaptive Control and Hydrodynamic Simulation," Journal of Marine Science and Engineering, vol. 10, no. 1, doi: 10.3390/jmse10010083.

[6] L. Hu, M. Zhang, X. Yu, Z.-M. Yuan, and W. Li, "Real-time control of ship's roll motion with gyrostabilisers," Ocean Engineering, vol. 285, p.

[7] M.-C. Fang, Y.-Z. Zhuo, and Z.-Y. Lee, "The application of the self-tuning neural network PID controller on the ship roll reduction in random waves," Ocean Engineering - OCEAN ENG, vol. 37, pp. 529-538, 05/01 2010, doi: 10.1016/j.oceaneng.2010.02.013.

[8] X. Wu, Q. Liu, K. Zhang, and X. Xin, "Optimal-tuning of proportional-integral-derivative-like controller for constrained nonlinear systems and application to ship steering control," Journal of the Franklin Institute, vol. 355, no. 13, pp. 5667-5689, 2018.

[9] M. Palraj and P. Rajamanickam, "Motion control studies of a barge mounted offshore dynamic wind turbine using gyrostabilizer," Ocean Engineering, vol. 237, p. 109578, 2021.

[10] H. Takeuchi, K. Umemura, and S. Maeda, "Development of the Anti Rolling Gyro 375T (rolling stabilizer for yachts) using space control technology," Mitsubishi Heavy Industries Technical Review, vol. 48, no. 4, pp. 70-75, 2011.

[11] M. Taşkın, R. Guclu, and O. Ahan, H $\infty$ Optimal Control of DTMB 5415 Combatant Roll Motion with Active Fins. 2020, pp. 1-5.

[12] I. A. Jimoh, I. B. Küçükdemiral, and G. Bevan, "Fin control for ship roll motion stabilisation based on observer enhanced MPC with disturbance rate compensation," Ocean Engineering, vol. 224, p. 108706, 2021.

[13] M. Laurenza, G. Pepe, D. Antonelli, and A. Carcaterra, "Car collision avoidance with velocity obstacle approach: Evaluation of the reliability and performace of the collision avoidance maneuver," in 5th International Forum on Research and Technologies for Society and Industry: Innovation to Shape the Future, RTSI 2019 - Proceedings, 2019, pp. 465-470, doi: 10.1109/RTSI.2019.8895525.

[14] G. Pepe, M. Laurenza, D. Antonelli, and A. Carcaterra, "A new optimal control of obstacle avoidance for safer autonomous driving," in 2019 AEIT International Conference of Electrical and Electronic Technologies for Automotive, AEIT AUTOMOTIVE 2019, 2019, doi: 10.23919/EETA.2019.8804549.

[15] T. I. Fossen, Handbook of marine craft hydrodynamics and motion control. John Wiley & Sons, 2011.

[16] A. P. I. (API), "Design and Analysis of Stationkeeping Systems for Floating Structures ," Third ed: API RP2SK, 2015.

[17] G. Pepe, D. Antonelli, L. Nesi, and A. Carcaterra, "Flop: Feedback local optimality control of the inverse pendulum oscillations," in Proceedings of ISMA 2018 - International Conference on Noise and Vibration Engineering and USD 2018 - International Conference on Uncertainty in Structural Dynamics, 2018, pp. 93-106.

[18] M. Laurenza et al., "Surface Unmanned Multipurpose Research Marine Vehicle: SUNMARE Project," in Progress in Marine Science and Technology, 2022, vol. 6, pp. 522-529, doi: 10.3233/PMST220062.

[19] T. Irmak, V. Kotian, R. Happee, K. N. de Winkel, and D. M. Pool, "Amplitude and Temporal Dynamics of Motion Sickness," Frontiers in Systems Neuroscience, Original Research vol. 16, 2022.

[20] J. O'Hanlon and M. McCauley, "Motion Sickness Incidence as a Function of Vertical Sinusoidal Motion," Aerospace medicine, vol. 45, pp. 366-9, 05/01 1974.